Geophysical Prospecting

EAGE EUROPEAN ASSOCIATION OF GEOSCIENTISTS & ENGINEERS

Geophysical Prospecting, 2014 doi: 10.1111/1365-2478.12166

Sparsity-Aware Multiple Microseismic Event Localization Blind to the Source Time-Function

Hadi Jamali-Rad[2]*, Zijian Tang[1], Xander Campman[1], Alexander Droujinine[1] and Geert Leus[2]

[1]*Shell Global Solutions International B. V., and* [2]*the Delft University of Technology (TU Delft)*

ABSTRACT

We consider the problem of simultaneously estimating three parameters of multiple microseimic events, i.e., the hypocenter, moment tensor, and origin time. This problem is of great interest because its solution could provide a better understanding of reservoir behavior and can help to optimize the hydraulic fracturing process. The existing approaches employing spatial source sparsity have advantages over traditional full-wave inversion-based schemes; however, their validity and accuracy depend on the knowledge of the source time-function, which is lacking in practical applications. This becomes even more challenging when multiple microseimic sources appear simultaneously. To cope with this shortcoming, we propose to approach the problem from a frequency-domain perspective and develop a novel sparsity-aware framework that is blind to the source time-function. Through our simulation results with synthetic data, we illustrate that our proposed approach can handle multiple microseismic sources and can estimate their hypocenters with an acceptable accuracy. The results also show that our approach can estimate the normalized amplitude of the moment tensors as a by-product, which can provide worthwhile information about the nature of the sources.

Key words: Microseismics, Parameter estimation, Sparse reconstruction.

INTRODUCTION

Microseismic event monitoring is a fundamental problem that has received an upsurge of attention in literature. Parameter estimation of microseismic events (also called sources), i.e., estimating their hypocenter, moment tensor components, and origin-time, provides important information about volumetric stress/strain and failure mechanisms in reservoirs Baig and Urbancic (2010). This parameter estimation is also of special interest for monitoring earthquakes in seismically active areas Scognamiglio, Tinti, and Michelini (2009), for mitigating hazards in mining operations Gibowicz (2009), and for monitoring and assessing the amount of adjustments during and after a hydraulic fracturing process Droujinine, Winsor, and Slauenwhite (2012), to name a few.

Most of the previous studies in this context are based on fast inversion or full-wave inversion Li, Zhang, and Toksöz (2009), which suffer from the following main shortcomings: they cannot provide a simultaneous estimate of the three source parameters, they are mostly single-source algorithms, and they are not real-time because of the large bulk of measured seismic traces they have to deal with. Moreover, most of these methods include iterative algorithms that are sensitive to an appropriate initialization. All these issues motivated researchers to think about grid-based approaches Lee *et al.* (2010) where run-time measurement traces are compared with a pre-constructed database of seismic traces also known as a dictionary. On the other hand, constructing such a dictionary requires extra computational effort.

A deeper look into the grid-based problem reveals that (in a single-source setup) the source hypocenter is unique in the spatial domain and thus can be represented by a 1-sparse

*E-mail: {h.jamalirad}@tudelft.nl

(containing only one non-zero element) vector. This motivated the use of compressive sampling Donoho (2006) to recover the hypocenter of the source using a few measurements by solving an ℓ_1-norm minimization problem. This idea illustrated promising results for the first time in Cevher, Durate, and Baraniuk (2009) for localization in a signal processing context and in some subsequent studies on multi-source localization (Feng *et al.* 2012; Jamali-Rad and Leus 2013; Jamali-Rad, Ramezani, and Leus 2014), where multiple sources could occur at the same time and the received signals could not be decomposed according to their respective sources.

Recently, in a geophysical context, similar ideas have been employed to simultaneously recover the aforementioned three source parameters. In Rodriguez, Sacchi, and Gu (2012a), a sparse representation framework is proposed to model the microseismic source activities, and it is shown that employing sparse reconstruction techniques makes it possible to jointly estimate the source parameters with acceptable accuracy. In Rodriguez, Sacchi, and Gu (2012b), the same ideas as in Rodriguez, Sacchi, and Gu (2012a) are presented; however, by applying a further compression step (leading to a compressive sensing framework) it is shown that the proposed framework in Rodriguez, Sacchi, and Gu (2012a) becomes real-time and considerably less demanding in terms of computational cost. In Rodriguez and Sacchi (2013), compressive sensing is combined with migration-based techniques to simultaneously estimate the three source parameters. The resulting migration-based problem is then analyzed in the frequency domain. Notably, handling multiple microseismic sources has not been explicitly considered in (Rodriguez, Sacchi, and Gu 2012a; Rodriguez, Sacchi, and Gu 2012b; and Rodriguez and Sacchi 2013). We should further emphasize that handling a multi-source setup in the frequency domain, as we develop here, calls for a structured approach, which has not been derived in Rodriguez and Sacchi (2013).

The validity of the sparsity-aware approach presented by (Rodriguez, Sacchi, and Gu 2012a; Rodriguez, Sacchi, and Gu 2012b) relies heavily on whether a good estimation of the source time-function is available. More specifically, the approach of (Rodriguez, Sacchi, and Gu 2012a; Rodriguez, Sacchi, and Gu 2012b) only works if there exists one (or more) source(s) with a source time-function exactly the same as the one used to construct the dictionary. Practically speaking, this is a rather hard constraint because different sources have different natures and thus different source time-functions; this limits the application domain of this approach. The same holds for Rodriguez and Sacchi (2013) when it comes to handling multiple sources. To overcome this limitation, in this paper, we propose a novel idea to eliminate this crucial need for the knowledge of the source time-function by approaching the problem from the frequency domain. We show that our proposed approach is capable of estimating the hypocenter of multiple microseismic sources with high accuracy. The results are also promising in the sense that they motivate a further study to extract the other parameters, i.e., exact moment tensor components and source origin-times.

This paper is structured as follows. In Section II, we explain the acquisition setup and signal model under consideration. Section III briefly reviews the proposed approach of (Rodriguez, Sacchi, and Gu 2012a; and Rodriguez, Sacchi, and Gu 2012b). Next, our proposed frequency-domain approach (blind to the source time-function) is explained. Section IV illustrates several simulation results, and finally, this paper is summarized in Section V by discussing a few possible future research directions.

ACQUISITION GEOMETRY AND SIGNAL MODEL

An area of interest (normally 3-D, in x, y, and z), which is prone to microseismic events (e.g., fractures), is discretized into N grid points. These grid points are the potential candidates for the hypocenter of a microseismic event. The area of interest lies somewhere underground in the vicinity of a well. Traditionally, the grid structure is chosen to be a uniform one with a fixed grid spacing, even though a non-uniform structure (depending on the properties of the area) can also be considered. The other components of our acquisition system are the geophones used to measure the displacements in 3-D; we consider L of them in total. Geophones can be arranged in the form of multiple linear (horizontal or vertical) arrays in the traditional way, or they can be more arbitrarily distributed, i.e., either on the surface or buried underground.

The phenomena of interest, as explained earlier, are microseismic events, which we model by a time-dependent moment tensor $\mathbf{M}(t)$. Quite often, it is assumed in seismology that the time variation of the moment tensor can be separated from its geometry (Madariaga 2007; Aki and Richards 2002), which leads to $\mathbf{M}(t) = \mathbf{M}s(t)$ with $s(t)$ defined as the source time-function, and for a general seismic source (three orthogonal linear dipoles), $\mathbf{M}$ is specified by a symmetric tensor of rank 2 given by Madriaga (2007)

$$\mathbf{M} = \begin{bmatrix} m_{xx} & m_{xy} & m_{xz} \\ m_{yx} & m_{yy} & m_{yz} \\ m_{zx} & m_{zy} & m_{zz} \end{bmatrix}. \tag{1}$$

Now, by considering the six diagonal and upper diagonal elements of $\mathbf{M}$, the n-th component of the displacement at time t measured at a geophone located at $\mathbf{x}$ from a source located at $\boldsymbol{\zeta}$ can be computed by

$$u_n(\mathbf{x},t) = \sum_{pq} m_{pq}(t) * \frac{\partial}{\partial \boldsymbol{\zeta}_q} G_{np}(\mathbf{x},\boldsymbol{\zeta},t,\tau) = \sum_{pq} m_{pq}\, s(t) * \frac{\partial}{\partial \boldsymbol{\zeta}_q} G_{np}(\mathbf{x},\boldsymbol{\zeta},t,\tau), \quad (2)$$

where $\frac{\partial}{\partial \zeta_q} G_{np}(.)$ denotes the spatial derivative of the Green's function characterizing the medium between the n-th component of the geophone and the p-th component of the source hypocenter with respect to the q-th component of the source hypocenter. Notably, the n, p, and q indices denote x, y, or z. Further, τ denotes the source origin-time, and $*$ stands for the time-domain convolution. We consider up to K simultaneous microseismic sources to appear within each measurement time interval. As a convention, from now on, we simply use the term source instead of microseismic event/source.

SPARSITY-AWARE PARAMETER ESTIMATION

The idea behind involving sparse reconstruction is the fact that, in practice, the number of simultaneous sources K is much smaller than the total number of grid points N. In order to incorporate this spatial source sparsity, the received time-domain displacement traces at the different geophones from all possible candidate source hypocenters (grid points) are simulated (or measured) to construct a dictionary of displacement traces. In a dictionary learning context, this is sometimes called the "training phase". Next, in the so-called "run-time phase", the real-time received displacements are compared with the content of the pre-constructed dictionary to estimate the unknown parameters of interest, i.e., moment tensor components, source hypocenter, and source origin-time. To carry out this comparison, the embedded sparsity is promoted by introducing the ℓ_1-norm and by taking into account the group structure of the variables involved. The resulting reconstruction problem will then be solved using the group least absolute shrinkage and selection operator (G-LASSO) Yuan and Lin (2006) or alternatively with the block orthogonal matching pursuit (BOMP) Eldar, Kuppinger, and Bolcskei (2010). This method has already been studied by (Rodriguez, Sacchi, and Gu 2012a; Rodriguez, Sacchi, and Gu 2012b) for our application of interest; however, their approach suffers from the following practical limitation.

Motivation: In (Rodriguez, Sacchi, and Gu 2012a; Rodriguez, Sacchi, and Gu 2012b), the dictionary is highly dependent on the source time-function $s(t)$, which means that the source in the run-time phase should have the same source time-function as the one which is considered to construct the dictionary denoted as $s_0(t)$. The situation gets even worse for the multi-source case where $s_k(t) = s_0(t)\ \forall k$ (with $s_k(t)$ being the source time-function of the k-th source) should hold to avoid poor results. This is difficult to achieve in practice as the sources might have a different nature and thus a different $s(t)$. This motivated us to think about a novel multi-source sparsity-aware framework which does not rely on the knowledge of $s(t)$, or is blind to $s(t)$. Interestingly, a solution exists and can be developed by approaching the problem from the frequency domain as explained in the following.

Let us start by looking at the frequency-domain representation of equation 2. To do so, we sample the time-domain displacement traces with a sampling frequency of F_s ($F_s = 1/T_s$, with T_s being the sampling interval) and take a discrete Fourier transform (DFT) of length N_t to obtain

$$\tilde{u}_n(\mathbf{x},\omega) = \sum_{pq} m_{pq} \frac{\partial}{\partial \boldsymbol{\zeta}_q} \tilde{G}_{np}(\mathbf{x},\boldsymbol{\zeta},\omega)\, \tilde{s}(\omega)\, e^{j\omega\tau}, \quad (3)$$

where $\omega = 2\pi\, F_s\, i/N_t$ with $i = 0, 1, \ldots, N_t - 1$, and $\tilde{(.)}$ emphasizes that we deal with a frequency-domain representation. Note that the time convolution is converted to a (sample by sample) product in the frequency domain. Now, we take N_f frequencies ω_f, with $f = 1, \ldots, N_f$ from the set of N_t frequencies. This allows us to construct the matrix form for different f's given by

$$\underbrace{\begin{bmatrix} \tilde{u}_x(\mathbf{x},\omega_f) \\ \tilde{u}_y(\mathbf{x},\omega_f) \\ \tilde{u}_z(\mathbf{x},\omega_f) \end{bmatrix}}_{\tilde{\mathbf{u}}(\mathbf{x},\omega_f)} = \underbrace{\tilde{s}_0(\omega_f) \begin{bmatrix} \frac{\partial}{\partial\zeta_x}\tilde{G}_{xx} & \frac{\partial}{\partial\zeta_y}\tilde{G}_{xx} & \cdots & \frac{\partial}{\partial\zeta_z}\tilde{G}_{xz} \\ \frac{\partial}{\partial\zeta_x}\tilde{G}_{yx} & \frac{\partial}{\partial\zeta_y}\tilde{G}_{yx} & \cdots & \frac{\partial}{\partial\zeta_z}\tilde{G}_{yz} \\ \frac{\partial}{\partial\zeta_x}\tilde{G}_{zx} & \frac{\partial}{\partial\zeta_y}\tilde{G}_{zx} & \cdots & \frac{\partial}{\partial\zeta_z}\tilde{G}_{zz} \end{bmatrix}}_{\tilde{\boldsymbol{\Psi}}(\mathbf{x},\boldsymbol{\zeta},\omega_f)} \times \underbrace{\begin{bmatrix} m_{xx} \\ m_{xy} \\ \vdots \\ m_{zz} \end{bmatrix} \frac{\tilde{s}(\omega_f)}{\tilde{s}_0(\omega_f)}\, e^{j\omega_f\tau}}_{\tilde{\mathbf{m}}(\boldsymbol{\zeta},\omega_f,\tau)}, \quad (4)$$

where the argument $(\mathbf{x}, \boldsymbol{\zeta}, \omega_f)$ is omitted for the Green's functions to simplify the notation.

Looking at the formulation in equation (4), we see an important phenomenon in the frequency domain where both the source origin-time and the source time-function (represented

at ω_f) are translated into two (complex) constant factors. For the sake of consistency with the time-domain approach presented by Rodriguez, Sacchi, and Gu (2012a) and Rodriguez, Sacchi, and Gu (2012b), we also keep $\tilde{s}_0(\omega_f)$ in $\tilde{\boldsymbol{\Psi}}(\mathbf{x}, \boldsymbol{\zeta}, \omega_f)$ and thus in our dictionary. The contribution of the origin-time, however, can easily be accommodated in the newly defined sub-vector of interest $\tilde{\mathbf{m}}(\boldsymbol{\zeta}, \omega_f, \tau)$. Next, we expand equation (4) for L geophones located at $\mathbf{x}_1, \ldots, \mathbf{x}_L$ and consider K sources located at $\boldsymbol{\zeta}_1, \ldots, \boldsymbol{\zeta}_K$ to have

$$\begin{aligned}\tilde{\mathbf{u}}(\omega_f) &= [\tilde{\mathbf{u}}_1(\omega_f)^T, \ldots, \tilde{\mathbf{u}}_L(\omega_f)^T]^T \\ &= \sum_{k=1}^{K} \underbrace{[\tilde{\boldsymbol{\Psi}}_1(\boldsymbol{\zeta}_k, \omega_f)^T, \tilde{\boldsymbol{\Psi}}_2(\boldsymbol{\zeta}_k, \omega_f)^T, \ldots, \tilde{\boldsymbol{\Psi}}_L(\boldsymbol{\zeta}_k, \omega_f)^T]^T}_{\tilde{\boldsymbol{\Psi}}(\boldsymbol{\zeta}_k, \omega_f)} \\ &\quad \times \tilde{\mathbf{m}}(\boldsymbol{\zeta}_k, \omega_f, \tau_k), \end{aligned} \tag{5}$$

where $(.)^T$ denotes the transposition operator on a vector or a matrix, $\tilde{\boldsymbol{\Psi}}_l(\boldsymbol{\zeta}_k, \omega_f) = \tilde{\boldsymbol{\Psi}}(\mathbf{x}_l, \boldsymbol{\zeta}_k, \omega_f)$ with $\mathbf{x}_l$ being the hypocenter of the l-th geophone, and $\tilde{\mathbf{u}}_l(\omega_f) = \tilde{\mathbf{u}}(\mathbf{x}_l, \omega_f)$ is a 3×1 frequency-domain displacement vector observed at the l-th geophone; accordingly, $\tilde{\mathbf{u}}(\omega_f)$ is of size $3L \times 1$. Again, similar to the time-domain approach, the next step will be discretizing the space into N grid points as the candidate points for the hypocenter of the K sources, which helps us to expand equation (5) by considering all the grid points and constructing a linear set of equations as

$$\tilde{\mathbf{u}}(\omega_f) = \underbrace{[\tilde{\boldsymbol{\Psi}}_1(\omega_f), \tilde{\boldsymbol{\Psi}}_2(\omega_f), \ldots, \tilde{\boldsymbol{\Psi}}_N(\omega_f)]}_{\tilde{\boldsymbol{\Psi}}(\omega_f)} \tilde{\mathbf{m}}(\omega_f), \tag{6}$$

where $\tilde{\boldsymbol{\Psi}}_n(\omega_f) = \tilde{\boldsymbol{\Psi}}(\boldsymbol{\eta}_n, \omega_f)$ with $\boldsymbol{\eta}_n$ being the location of the n-th grid point and

$$\tilde{\mathbf{m}}(\omega_f) = [\tilde{\mathbf{m}}_1(\omega_f)^T, \tilde{\mathbf{m}}_2(\omega_f)^T, \ldots, \tilde{\mathbf{m}}_N(\omega_f)^T]^T, \tag{7}$$

is of size $6N \times 1$ where $\tilde{\mathbf{m}}_n(\omega_f) = \mathbf{0}$ unless there is a source on $\boldsymbol{\eta}_n$. Our parameters of interest can then be obtained by solving equation (6) for $\tilde{\mathbf{m}}(\omega_f)$.

Notable Remarks:

(i) The fact that we accommodate the source origin-time-related constants ($e^{j\omega_f\tau}$) in $\tilde{\mathbf{m}}(\omega_f)$ describes that the dictionary is normally constructed with a zero-origin-time source, and thus, the effect of the origin-time will appear in $\tilde{\mathbf{m}}(\omega_f)$ in the form of a complex constant.

(ii) By looking at equations (4) and (6), we observe that the dictionary can be constructed with a source with even unknown $s_0(t)$ (equivalently, $\tilde{s}_0(\omega)$); whatever the source-time function in the real-time measurements is, its proportional effect in the form of a constant $\tilde{s}_k(\omega_f)/\tilde{s}_0(\omega_f)$ will appear in $\tilde{\mathbf{m}}(\omega_f)$. This is the key point of the frequency-domain approach, which allows us to design our (blind to $s(t)$) approach.

(iii) This framework provides the flexibility to handle different source origin-times for different sources and different source time-functions. This also has the advantage that making a huge super-dictionary as the one proposed by Rodriguez, Sacchi, and Gu (2012a) is no longer necessary and the converted frequency-domain data will be handled more efficiently, as will be explained in the following.

(iv) The downside is that the source origin-time and the source time-function effects will appear as constant factors in $\tilde{\mathbf{m}}(\omega_f)$, which makes it hard to extract them.

A simple possibility to estimate our desired parameters is to confine ourselves to one specific frequency and solve equation (6) using a G-LASSO type of estimator similar to the case of the time-domain approach; however, this approach will be naive as we do not really exploit all the information (encoded in different frequencies) available. Therefore, the important question is how to incorporate all the frequencies (the ω_f's) to make a much better estimation?

Notably, different from classical G-LASSO and other similar estimators, here we have different dictionaries $\tilde{\boldsymbol{\Psi}}(\omega_f)$ for different frequencies, which means that our different measurement vectors $\tilde{\mathbf{u}}(\omega_f)$ characterize different vectors of interest $\tilde{\mathbf{m}}(\omega_f)$. A pictorial view of the estimation problem at hand is depicted in Fig. 1. The key observation that should be taken into account to handle this problem is that even though the $\tilde{\mathbf{m}}(\omega_f)$'s contain different values (due to $\tilde{s}(\omega_f)$ and $e^{j\omega_f\tau}$), they share the same sparsity support, i.e., they are zero or non-zero at similar indices (groups). These groups are shown in Fig. 1 using similar colors within the $\tilde{\mathbf{m}}(\omega_f)$'s and across the corresponding subsections of the $\tilde{\Psi}(\omega_f)$'s. In order to deal with this situation, we propose the following estimator (basically an extension of the estimator proposed in (Tang, Blacquiere, and Leus 2011) for wideband beamforming "and" the G-LASSO employed in Rodriguez, Sacchi, and Gu (2012a) and Rodriguez, Sacchi, and Gu (2012b)) and we call it multi dictionary G-LASSO (MDG-LASSO) given by

$$\begin{aligned}\hat{\Theta}_{MDG-LASSO} = \arg\min_{\Theta} &\sum_{f=1}^{N_f} \|\tilde{\mathbf{u}}(\omega_f) - \tilde{\boldsymbol{\Psi}}(\omega_f)[\boldsymbol{\Theta}]_{:,f}\|_2^2 \\ &+\lambda \sum_{n=1}^{N} \|[\boldsymbol{\Theta}]_{6(n-1)+1:6n,:}\|_2, \end{aligned} \tag{8}$$

where $\boldsymbol{\Theta} = [\tilde{\mathbf{m}}(\omega_1), \ldots, \tilde{\mathbf{m}}(\omega_{N_f})]$. The first term on the right-hand-side of equation (8) is the least squares part, which minimizes the error for the different frequencies, and the

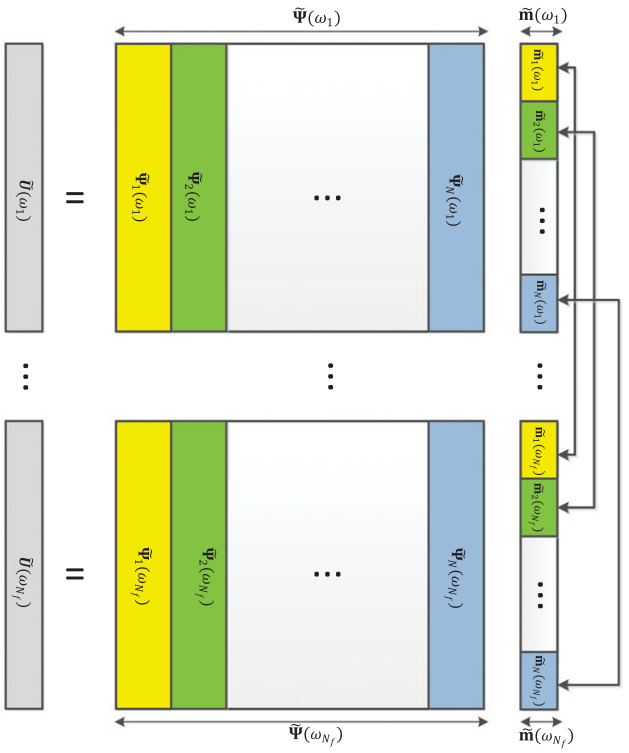

Figure 1 Illustration of linear sets of equations in different ω_f's. $\tilde{\mathbf{m}}(\omega_f)$'s share a common sparsity support and also have the same group structure that helps to propose a proper estimation approach.

second term enforces our specific group sparsity. It is worth pointing out that an analysis of the algorithms to solve equation (8) is outside the scope of this paper, and here we restrict ourselves to standard interior-point convex optimization tools such as CVX (CVX Research Inc. 2012) to solve the problem. Based on the discussions presented in Chen and Huo (2006) for a related concept, incorporating all the frequencies within equation (8) will result in a gain in terms of identifiability compared with simply considering a single frequency, as is also corroborated by our simulation results in Section IV. To sum up, we would like to highlight that the proposed MDG-LASSO estimator takes into account three important features of the problem at hand, namely, the group sparsity in the estimated vectors, the common sparsity support among them, and the fact that the model consists of different dictionaries for different measurements.

EVALUATION USING SYNTHETIC DATA

In this section, we investigate the performance of the proposed algorithms in terms of positioning root-mean-squared error

Table 1 Velocity profile

Layers	z margins (m)	v_p (m/s)	v_s (m/s)	ρ
Layer 1	−2920	5326	3286	2200
Layer 2	−3125	4968	2985	2200
Layer 3	−9000	4487	2768	2200

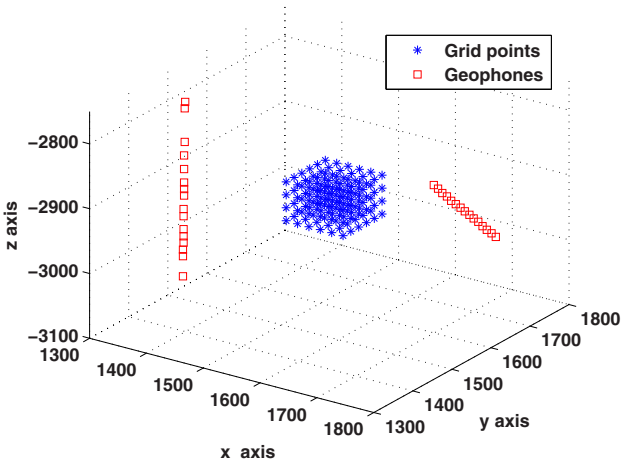

Figure 2 Acquisition setup

(PRMSE) and probability of detection (P_d) against signal-to-noise ratio (SNR), where the noise on the measured displacements is considered a band-limited additive white Gaussian noise occurring within the bandwidth of $\tilde{s}(\omega)$. We consider a three-layer elastic medium with different velocities in each layer. The velocity profile model can be found in Table 1 where primary-wave velocity, shear-wave velocity, and density are respectively denoted by v_p, v_s, and ρ. The synthetic data are generated using a MATLAB software package based on ray-tracing in order to compute the Green's functions for a full moment tensor source model in a multi-layer 3-D medium.

The acquisition setup is shown in Fig. 2. As can be seen, $L = 31$ geophones arranged in two arrays (vertical and horizontal) are employed to measure the displacement traces. This can also be done using a single array of geophones. Investigating the effect of different geophone geometries is omitted in this paper due to limited space. The area of interest is uniformly discretized into $N = 144$ grid points as shown in Fig. 2 with a grid spacing of $\Delta = 20$ m in three dimensions. The adopted moment tensor model is a six-component vector (considering diagonal and upper diagonal elements of $\mathbf{M}$) with fixed components ($\mathbf{m} = [0.7, 1, 0.5, 0.9, 0.7, 0.8]^T$) for all the sources. Note that this can be even different for all the sources and it will not affect our performance at all, as long as none

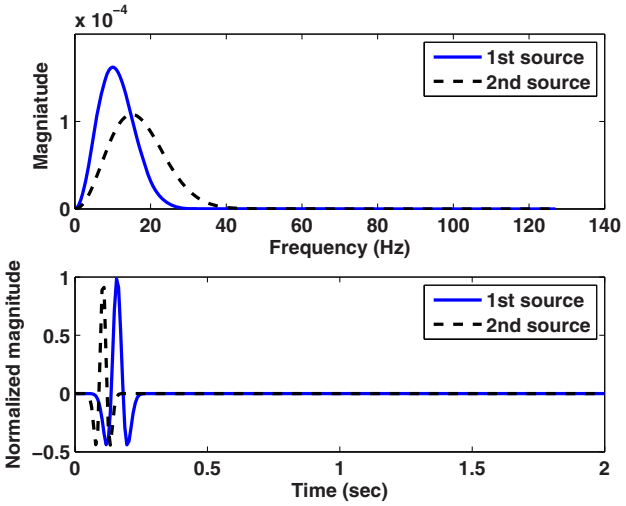

Figure 3 Two different $s(t)$'s

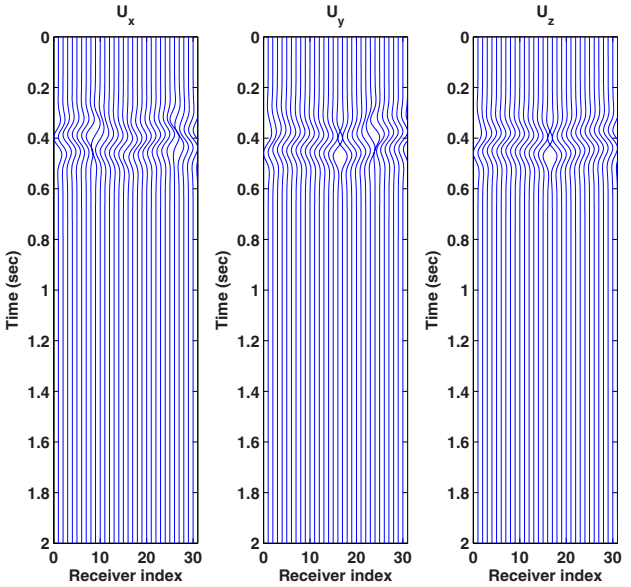

Figure 4 Received displacements

of these components is significantly larger/smaller than the others. In order to prove that our approach is blind to $s(t)$, we consider two different $s(t)$'s as shown in Fig. 3, and we use the first one ($s_0(t)$) to construct the dictionaries and the second one for the real-time measurements (without loss of generality $s_k(t) = s(t) \neq s_0(t), \forall k$). As depicted in Fig. 3, these functions are chosen to be the well-known Ricker wavelets with peak frequencies at 10 Hz and 15 Hz, respectively.

Another parameter, which is clear from Fig. 3, is the measurement interval of 2 seconds corresponding to $N_t = 256$; thus, $F_s = 256/2 = 128$ Hz. This is obviously larger than twice the maximum frequency of the sources (approximately 40 Hz according to Fig. 3) to satisfy the Nyquist criterion. Note that the source origin-times can be integer or even non-integer multiples of T_s and their values do not affect the performance. In our simulations, origin-times are chosen randomly within a range of $[0,\ 9]\,T_s$. Moreover, we consider only $N_f = 18$ frequencies ($2\pi[1, 3, 5, \ldots, 35]^T$), which means we will have 18 dictionaries $\tilde{\Psi}(\omega_f)$, each of size $3L(= 93) \times 6N(= 864)$. Notably, another design consideration that has carefully been taken into account is that the length of the time-bin should be much larger than the rule-of-thumb maximum possible delay of the received displacement traces. This is to ensure that the latest displacement arrivals will be covered by measurements.

We consider up to $K = 3$ sources occurring simultaneously (during one measurement interval). Most of the simulations, whenever they do not illustrate a single snapshot, are averaged over $P = 50$ independent Monte Carlo runs, where in each run, the sources are deployed on different random locations (hypocenters). Increasing P will result in smoother curves. For the sake of comparison, in addition to the MDG-LASSO, we also consider a G-LASSO for which only an appropriate single frequency (here $f = 15$) is taken into account. Another possibility is to average the results of this G-LASSO over all the frequencies, which is not illustrated here. Averaging over different frequencies will not provide a much better result because, in many single frequencies, the estimations are poor, especially for the case of multiple microseismic sources.

In order to quantify the performance we consider two different metrics

- First, the PRMSE defined by

$$\text{PRMSE} = \sqrt{\frac{1}{PK}\sum_{p=1}^{P}\sum_{k=1}^{K} e_{k,p}^2}, \tag{9}$$

where $e_{k,p}$ represents the distance between the real hypocenter of the k-th source and its estimated hypocenter at the p-th Monte Carlo trial.

- Second, the probability of detection (P_d) where a source is considered to be detected if it is estimated to be within a sphere with radius $\sqrt{3} \times \Delta$ around its real hypocenter with Δ defined earlier.

Let us start with a single source located at $(1525, 1585, -2900)$ corresponding to our grid point with index 62. The displacements measured at the 31 geophones are plotted in Fig. 4. The SNR is set to 30 dB. The result of our proposed parameter estimation algorithm is illustrated

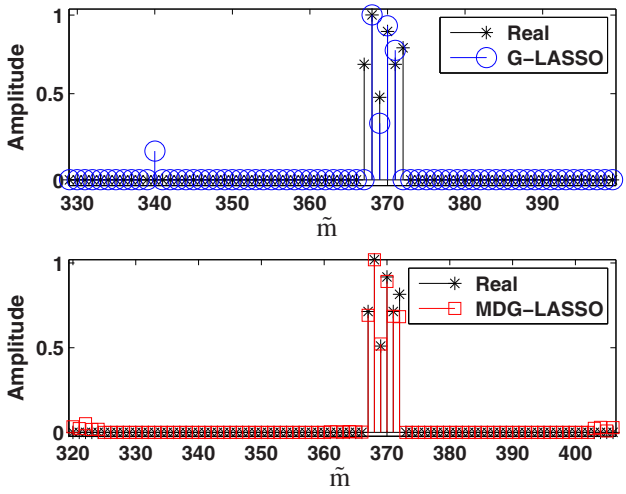

Figure 5 Estimation of $\tilde{\mathbf{m}}$ for single source; selected indices and corresponding amplitudes compared with their real values.

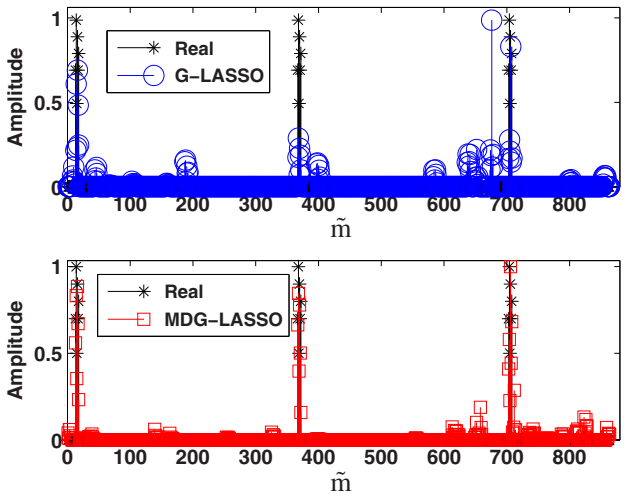

Figure 6 Estimation of $\tilde{\mathbf{m}}$ for multiple sources; selected indices and corresponding amplitudes compared with their real values.

in Fig. 5 where, as can be seen, both G-LASSO and MDG-LASSO activate the correct group of indices in $\tilde{\mathbf{m}}$ (i.e., $61 \times 6 + 1 = 367, \cdots, 61 \times 6 + 6 = 372$). Note that, for a better visualization, the amplitudes of the estimated moment tensors contained in $\hat{\mathbf{\Theta}}_{MDG-LASSO}$ are normalized, and we plot $\tilde{\mathbf{m}} = \sum_{f=1}^{N_f} \tilde{\mathbf{m}}(\omega_f)$ for MDG-LASSO. It is notable that, in contrast to G-LASSO, the moment tensors estimated by MDG-LASSO are just scaled versions of the real moment tensors. We would like to emphasize that, according to Aki and Richards (2002), the normalized moment tensors contain important information about the nature of the sources, and thus, this information will be extracted using our proposed approach. Further, this is also a promising point as it motivates a further post-processing step to possibly extract the exact moment tensor values as well as origin-times from the estimated amplitudes. This topic is left as future work.

Fig. 6 is similar to Fig. 5, but it presents the case of $K = 3$ sources with different origin-times. The other two sources are located at $(1545, 1505, -2880)$ and $(1560, 1525, -2940)$, where the latter is off-grid (close to the grid point with index 118) and the former is on the grid point with index 3. As can be seen from the activated indices, while MDG-LASSO can easily handle the three sources, the (single-frequency) G-LASSO does not show an acceptable performance with a stable estimation. This is because, only with 91 rows (measurements) in $\tilde{\mathbf{\Psi}}(\omega_{15})$, it is impossible to accurately reconstruct a sparse vector of interest with $3 \times 6 = 18$ non-zero elements corresponding to the three sources. This issue is basically related to the concept of sparse reconstruction, and the interested reader

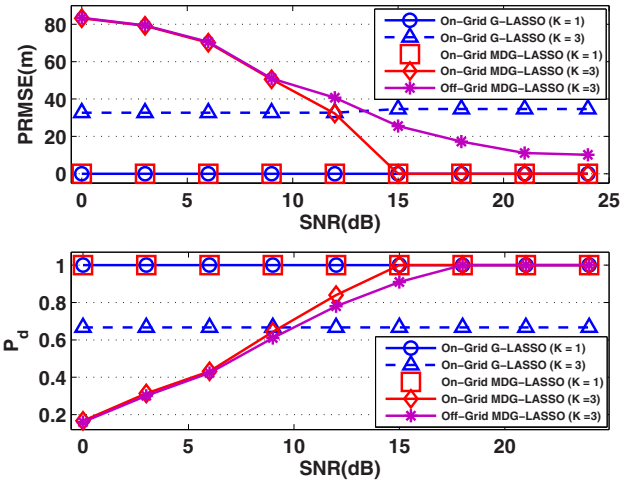

Figure 7 Proposed approach; localization and detection performances versus. SNR for $K = 1$ and $K = 3$ on-grid and off-grid sources.

is referred to Donoho (2006). The above result corroborates the idea that incorporating all the frequencies at the same time with our proposed MDG-LASSO estimator significantly improves the overall estimation performance. Note that, for the third source (closest to the grid point with index 118), the effect of being off-grid appears as a few other side groups of indices being activated with considerably smaller amplitudes compared with the correct group, i.e., the group corresponding to the grid point with index 118. This means that, even in the case of off-grid sources, at least the closest grid points are usually distinguishable.

Finally, Fig. 7 depicts the performance of the proposed approach against SNR for $K = 1$ and $K = 3$ sources

with $P = 50$ for both on-grid and off-gird sources. In the on-grid case, for a single source, both G-LASSO and MDG-LASSO (while they are blind to $s(t)$) can attain an excellent performance in terms of both PRMSE and P_d within a reasonably large span of SNRs [0, 24] dB. However, the effect of the proposed modified framework to incorporate all the frequencies at the same time shows its effect when the number of sources is increased. Interestingly, for $K = 3$, the (single-frequency) G-LASSO cannot attain an acceptable PRMSE and P_d performance even for high SNRs. Quite the opposite, the MDG-LASSO attains a perfect detection performance and zero hypocenter estimation error for SNRs above 15 dB. However, as can be seen, if we consider off-grid sources and only stick to finding the closest grid points, the performance of MDG-LASSO will be degraded in terms of both accuracy and detection performance.

DISCUSSION

In this paper, we confine ourselves to finding the closest grid points to the off-grid sources, although there might be a possibility to derive the relationship between the hypocenter of an off-grid source and its corresponding received displacements. In that case, techniques similar to the ones proposed in Jamali-Rad and Leus (2013) can be employed to devise a two-step approach where, in the first step, the closest grid points to the off-grid sources are found, and in the next step, their grid mismatch is recovered to find the real hypocenters. The simpler the medium (single-layer homogenous in the best case), the easier such relationships can be discovered. Moreover, currently, we only find the hypocenters of the sources and the normalized amplitudes of the moment tensors whereas according to our results, there is a possibility to further post-process the results and estimate the exact moment tensor amplitudes and the corresponding origintimes.

ACKNOWLEDGEMENTS

The authors would like to thank Shell Global Solutions International B.V. for financial support and for permitting to publish this paper. The authors would also like to thank Steve Oates and Renat Shigapov for their helpful discussions.

REFERENCES

Aki, K. and Richards, P. 2002. *Quantitative Seismology*, 2nd ed. Sausalito, CA: University Science Books.

Baig, A. and Urbancic, T. 2010. Microseismic moment tensors: A path to understanding fracture growth. *The Leading Edge* **29**, 320–324.

Cevher, V., Durate, M.F. and Baraniuk, R.G. Distributed target localization via spatial sparsity. Proceedings of European Signal Processing Conference, August 2009.

Chen, J. and Huo, X. 2006. Theoretical results on sparse representations of multiple-measurement vectors. *IEEE Transactions on Signal Processing* **54**, 4634–4643.

CVX Research Inc. 2012. CVX: MATLAB software for disciplined convex programming, version 2.0 beta. http://cvxr.com/cvx.

Donoho, D.L. 2006. Compressed sensing. *IEEE Transactions on Information Theory* **52**, 1289–1306.

Droujinine, A., Winsor, J. and Slauenwhite, K. Microseismic elastic full waveform inversion for hydraulic fracture monitoring. Proceedings of EAGE Conference and Exhibition, June 2012. Extended Abstracts, 2312–2316.

Eldar, Y., Kuppinger, P. and Bolcskei, H. 2010. Block-sparse signals: Uncertainty relations and efficient recovery. *IEEE Transactions on Signal Processing* **58**, 3042–3054.

Feng, C., Au, W.S.A., Valaee, S. and Tan, Z. 2012. Received signal strength based indoor positioning using compressive sensing. *IEEE Transactions on Mobile Computing* **11**, 1983–1993.

Gibowicz, Y. 2009. Seismicity induced by mining: Recent research. *Advances in Geophysics* **51**(6), 1–53.

Jamali-Rad, H. and Leus, G. 2013. Sparsity-aware multi-source TDOA localization. *IEEE Transactions on Signal Processing* **61**, 4874–4887.

Jamali-Rad, H., Ramezani, H. and Leus, G. 2014. Sparsity-Aware Multi-Source RSS Localization. *Elsevier Signal Processing* **101**, 174–191.

Lee, S.-J., Huang, B.-S., Liang, W.-T. and Chen, K.-C. 2010. Grid-based moment tensor inversion technique by using 3-D Greens functions database: A demonstration of the 23 October 2004 Taipei earthquake. *Terrestrial Atmospheric and Oceanic Sciences* **21**, 503–514.

Li, J., Zhang, H.K.H. and Toksöz, M.N. 2009. Focal mechanism determination using high frequency, full waveform information. *SEG Expanded Abstracts* **28**, 2312–2316.

Madariaga, R. 2007. Seismic source theory. *Treatise on Geophysics*, 59–82.

Rodriguez, I.V. and Sacchi, M.D. Microseismic source characterization combining compressive sensing with a migration based methodology. Proceedings of EAGE Conference and Exhibition, June 2013.

Rodriguez, I.V., Sacchi, M. and Gu, Y.J. 2012a. Simultaneous recovery of origin time, hypocentre location and seismic moment tensor using sparse representation theory. *Geophysical Journal International* **188**, 1188–1202.

Rodriguez, I.V., Sacchi, M. and Gu, Y.J. 2012b. A compressive sensing framework for seismic source parameter. *Geophysical Journal International* **191**, 1226–1236.

Scognamiglio, L., Tinti, E. and Michelini, A. 2009. Real-time determination of seismic moment tensor for the Italian region. *Bulletin of the Seismological Society of America 99*, 2223–2242.

Tang, Z., Blacquière, G. and Leus, G. 2011. Aliasing-free wideband beamforming using sparse signal representation. *IEEE Transactions on Signal Processing*, **59**, 3464–3469.

Yuan, M. and Lin, Y. 2006. Model selection and estimation in regression with grouped variables. *Journal of the Royal Statistical Society: Series B* **68**, 49–67.